scientific reports

Check for updates

OPEN

Electrically conductive lignin reinforced PAA/HA scaffolds with enhanced biological activity via polyelectrolyte multilayer coatings for tissue engineering applications

Caitriona Winters[1], Mario Culebras[2] & Maurice N. Collins[1,3,4]✉

In this study, a layer-by-layer deposition of poly(L-lysine) and hyaluronic acid (HA) as a polyelectrolyte multilayer (PEM) film on polyacrylic acid (PAA) /HA/ lignin (LIG) disc shaped scaffolds is presented to increase the biological activity of the scaffolds for tissue engineering applications. These scaffolds are electrically conductive via the introduction poly(3,4-ethylene dioxythiophene):hyaluronic acid (PEDOT:HA) nanoparticles (NPs), with a diameter of 10 mm and thickness of 3–4 mm. The multilayer film formation was confirmed through contact angle measurements, fluorescence microscopy and scanning electron microscopy (SEM) imaging. It was found that the PEM layers had the unexpected benefit of increased compression strength and decreased swelling as the layers tend to reinforce the struts of the scaffolds whilst possibly interfering with diffusion pathways. Importantly, results show statistically significant improved attachment and proliferation of L929 fibroblast cells on the surface of the scaffolds. Furthermore, the effect of varied PEDOT:HA NP addition was assessed and it was concluded that samples containing 1% (w/v) of nanoparticles exhibited a desirable balance between good mechanical characteristics, high conductivity, high cell adhesion and cell proliferation. These novel conductive PEM composite scaffolds offer future potential in biomedical applications such as tissue engineering, wound healing and biosensors.

Keywords Lignin, Hyaluronic acid, Tissue engineering, Polyelectrolyte, Coatings

Hyaluronic acid and acrylic acid are widely used in hydrogel synthesis, they are hydrophilic and biocompatible. Hyaluronic acid (HA) is a natural linear polysaccharide that has multiple reactive groups present in its molecular structure such as hydroxyl, carboxyl and acetamido, making it efficient for gel synthesis via various chemical, physical and autocrosslinking[1]. HA based gels generally have good dimensional stability, mechanical properties, biocompatibility and high swelling[2–7]. Polyacrylic acid (PAA) is a synthetic polymer also commonly used in the hydrogel synthesis, with PAA hydrogels possessing good biocompatibility, high water uptake capacity, pH sensitivity and ease of manufacture[8]. However, PAA lacks adhesive ligands for cell adhesion[9]. While HA does have specific cell binding sites, cell membranes may carry a negative surface charge which can repel or poorly interact with other negatively charged molecules unless specific ligands, bridging molecules or positively charged coatings are present[10,11]. In general, hydrogels are known to be highly tailorable materials that, through chemical modifications and careful material selection, can be imbued with properties such as biodegradability, biocompatibility, cellular attachment and improved mechanical characteristics[12–16].

Recent studies have investigated various solutions to enhance cell attachment and proliferation on scaffolds with poor bioactivity to improve their potential in tissue engineering applications. One solution that has yielded successful results is the use of bioactive coatings on the surface of inert scaffolds. For example, Arredondo et al. coated polyurethane meniscal scaffolds with fibronectin and found a significant improvement in the attachment and proliferation of mesenchymal stem cells on the scaffold's surface compared to uncoated samples, which could have a significant influence in the orthopaedic surgery of meniscal implants[17]. Similarly, Hum &

[1]Stokes Labs, Bernal Institute, School of Engineering, University of Limerick, Limerick, Ireland. [2]Institute of Material Science (ICMUV), University of Valencia, Valencia, Spain. [3]Health Research Institute, University of Limerick, Limerick, Ireland. [4]Research Ireland AMBER & BiOrbic Centres, University of Limerick, Limerick, Ireland. ✉email: Maurice.collins@ul.ie

Boccaccini found that coating a bioactive glass-based scaffold in collagen not only promoted cell viability and attachment but also the compressive strength of the scaffolds increased fivefold[18]. A layer-by-layer coating was also used by Bellucci et al. in which gelatin and chondroitin sulphate coated bioceramic scaffolds, significantly improving cell adhesion, proliferation and osteogenic activity, while also effecting the scaffolds microstructure and porosity[19]. Thus, the use of biocompatible coatings can significantly improve cell-scaffold interactions and scaffold performance which could in turn open a wider range of potential applications for tissue engineering in a clinical setting.

The use of polyelectrolyte multilayer (PEM) coatings is a method that has emerged as a versatile approach to improve cell adhesion for biomedical applications. These coatings can alter surface properties of a material to either promote or inhibit cell attachment, depending on the application[20]. PEM films can be tailored to improve cell integration on a scaffold, reduce bacterial infections and to reduce rejection of implants or scaffolds[21]. For instance, PEM coatings composed of poly(allylamine hydrochloride) and poly(4-vinylphenol) have shown inhibition of Staphylococcus epidermidis growth, while PAA and poly(allylamine hydrochloride) coatings reduced wear in orthopaedic devices[22]. The use of functional PEM coatings give the opportunity to combine the advantages of hydrogels such a hydrophilicity and biocompatibility with substrate properties such as stiffness and active binding sites to make them suitable for various medical applications[23]. PEMs of HA and poly-l-lysine (PLL) have been extensively studied for their potential in biomedical applications as cell-friendly coatings on biomaterials and devices[24]. Liu et al. used PEM coatings of (PLL) and HA on braided poly(l-lactide-co-caprolactone) scaffolds and found they yielded good biocompatibility with mesenchymal stem cells (MSCs) and had suitable mechanical properties for ligament tissue engineering[25]. PLL/HA films have also demonstrated potential as carriers for controlled release of growth factors from platelet lysates, promoting wound healing through enhanced granulation tissue formation, collagen deposition, and neovascularization[26].

Additionally, the addition of conductivity into scaffold materials can benefit its interactions with human tissues to encourage cell adhesion and proliferation as well as promoting its effectiveness in wound healing, tissue regeneration and physiological electric signalling[2,27,28]. Conductive hydrogel scaffolds offer significant advantages for cell functionality, as it enables the simulation of bioelectric signals found in tissues like cardiac, neural, and neuronal systems as well as enhancing cell proliferation, differentiation, and alignment which is crucial for creating functional regenerative tissue scaffolds[29,30]. Additionally, they provide opportunities for non-invasive, real-time monitoring of cell behaviour by leveraging electrical signals to evaluate cell health and differentiation[31,32]. There is however, a trade-off between conductivity with the addition of higher nanoparticle amounts and the stiffness and therefore the cell adhesion on scaffold materials and so an optimum configuration is important in order to maintain high conductivity without sacrificing mechanical or biological characteristics[33].

Previous work by the authors synthesised PAA/HA/LIG/PEDOT:HA NP scaffolds which were highly porous, conductive and absorbent, with high mechanical characteristics as a result of lignin incorporation[34]. Before the work completed by the current authors, only Wang et al. had incorporated PEDOT:HA NPs into a hydrogel scaffold. In that work PEDOT:HA NPs were utilised in a chitosan/gelatin hydrogel and results showed that, with the incorporation of the NPs, hydrogels had high cell adhesion (>71%), high mechanical characteristics and electrical conductivity was significantly increased. The sample in the study by Wang et al. that was most comparable to the work done by the current authors is the 2% PEDOT:HA sample, achieving a conductivity of 1.76×10^{-5} (S/cm) compared to a conductivity of 5.79×10^{-4} (S/cm) in the current author's study with 1% (w/v) of nanoparticles. The current materials of (PAA/HA/LIG), without nanoparticles, achieved a swelling degree of 114% which was considerably higher than values reported in the CHI/GEL scaffold without nanoparticles at around 32%. However, despite relatively high biocompatibility, swelling, conductivity and mechanical characteristics in these samples, cell adhesion and proliferation were poor for PAA/HA/LIG/PEDOT:HA scaffolds. Thus, this study aims to improve cell adhesion through the surface functionalisation of these scaffolds using polyelectrolyte multilayers (PEM)s of PLL and HA. The successful coating of the scaffolds was confirmed, and the samples were characterised mechanically, morphologically, biologically and via swelling tests to assess cell adhesion. An optimum coating configuration is selected, and NP concentration is varied within these samples to determine an optimum balance between electrical conductivity, mechanical characteristics and biocompatibility. The conductive NPs utilised here are a novel PEDOT:HA NP developed by the authors for enhanced biocompatibility[35].

Experimental section

Synthesis of nanoparticles

Nanoparticles were synthesised as previously reported by the current authors[35]. Firstly, 0.28 g Hyaluronic acid (HA; Shanghai Easier Development LTD, China) was dissolved in 40 mL 0.1 M hydrochloric acid solution (Analab, Ireland) and then 0.2 mL 3,4 Ethylenedioxythiophene (EDOT, 97%; Analab, Ireland) was added and stirred for 10 min. To avoid overheating, the solution was placed in an ice bath and ultrasonicated in a Branson Sonifier 450 for 10 min, and this results in a miniemulsion. This solution was then further sonicated and inserted in a reaction flask under stirring. Meanwhile, iron(III) p-toluenesulfonate hexahydrate (FeTos; Analab, Ireland) was stirred in DI water for 10 min to dissolve and was then added dropwise to the reaction flask to initiate polymerisation. After 1 h, 0.05 mL hydrogen peroxide (Analab, Ireland) was added and the solution was left stirring overnight. Once fully polymerised, nanoparticles were purified using centrifugation for three runs, redispersing in deionised (DI) water following each run. Then the nanoparticles were redispersed in 40 mL of DI water, sonicated for 20 min and then stored in a sealed flask.

Synthesis of hydrogels

Hydrogels were synthesised by the current authors as per[5]. First, 0.1 g of HA was added to a beaker containing 20 mL of DI water and stirred at 400 rpm overnight until the HA was fully dissolved. For samples containing

nanoparticles (NPs), 0.25 mL (1% w/v) of dispersed PEDOT:HA NPs were added to the solution, stirred and sonicated until a well-dispersed distribution was achieved. Then, 0.2 g lignosulfonate, 3.6 mL of acrylic acid (Analab, Ireland) and 0.03 g NN'-Bis(acryloyl)cystamine (BACA; Sigma Aldrich, Ireland) were added to the solution and stirred until dissolved. Finally, 0.03 g of ammonium persulfate (Sigma Aldrich, Ireland) was added and stirred until the sample was homogenous. The solution was then poured into a mould and placed in an oven for 3 h at 80 °C. Samples were also prepared containing no NPs for comparison. Following curing, the hydrogels were thoroughly washed and dried to remove any excess unreacted materials. Then they were frozen at -70 °C and transferred to the freezedryer (Alpha 1–4 LSCplus, CHRIST, Germany) for primary drying for 48 h and secondary drying until fully dried. Dry samples were cut into disc shaped scaffolds with a diameter of 10 mm and thickness of about 3–4 mm and were stored in a desiccator until coating.

Preparation and multilayer deposition of polyelectrolyte solutions

Initially, a 0.15 M NaCl solution was prepared in DI water. HA and PLL (Mw = 30,000–70,000 g/mol, Sigma Aldrich, Ireland) were dissolved separately in 0.15 M NaCl solutions at a concentration of 1 mg/mL. The pH was maintained at 6–6.5 for both solutions in order to keep HA negatively charged and PLL positively charged[36].

Dipping was used for multilayer formation on the hydrogel surface. The hydrogels were initially swollen at 37 °C in PBS (Sigma Aldrich, Ireland) for 48 h to obtain a constant weight. The hydrogels were then placed into the PLL solution for 7 min, then rinsed in PBS for 1 min and placed into the HA solution for 7 min and again rinsed in PBS for 1 min. This process was repeated until the desired amount of layer pairs was achieved and then finally dipped in PLL for a final time. The samples are labelled as $(PLL/HA)_n$-PLL, with n annotating the number of layer pair coatings. $(PLL/HA)_4$-PLL and $(PLL/HA)_8$-PLL) coated samples were synthesised, with $(PLL/HA)_0$ denoting uncoated scaffolds. Synthesis steps can be seen in Fig. 1.

FTIR

FTIR spectra of the hydrogels with polyelectrolyte multilayer films were obtained using the Spectrum 100 FTIR (PerkinElmer, USA) in the range 650–4000 cm^{-1} for 4 scans.

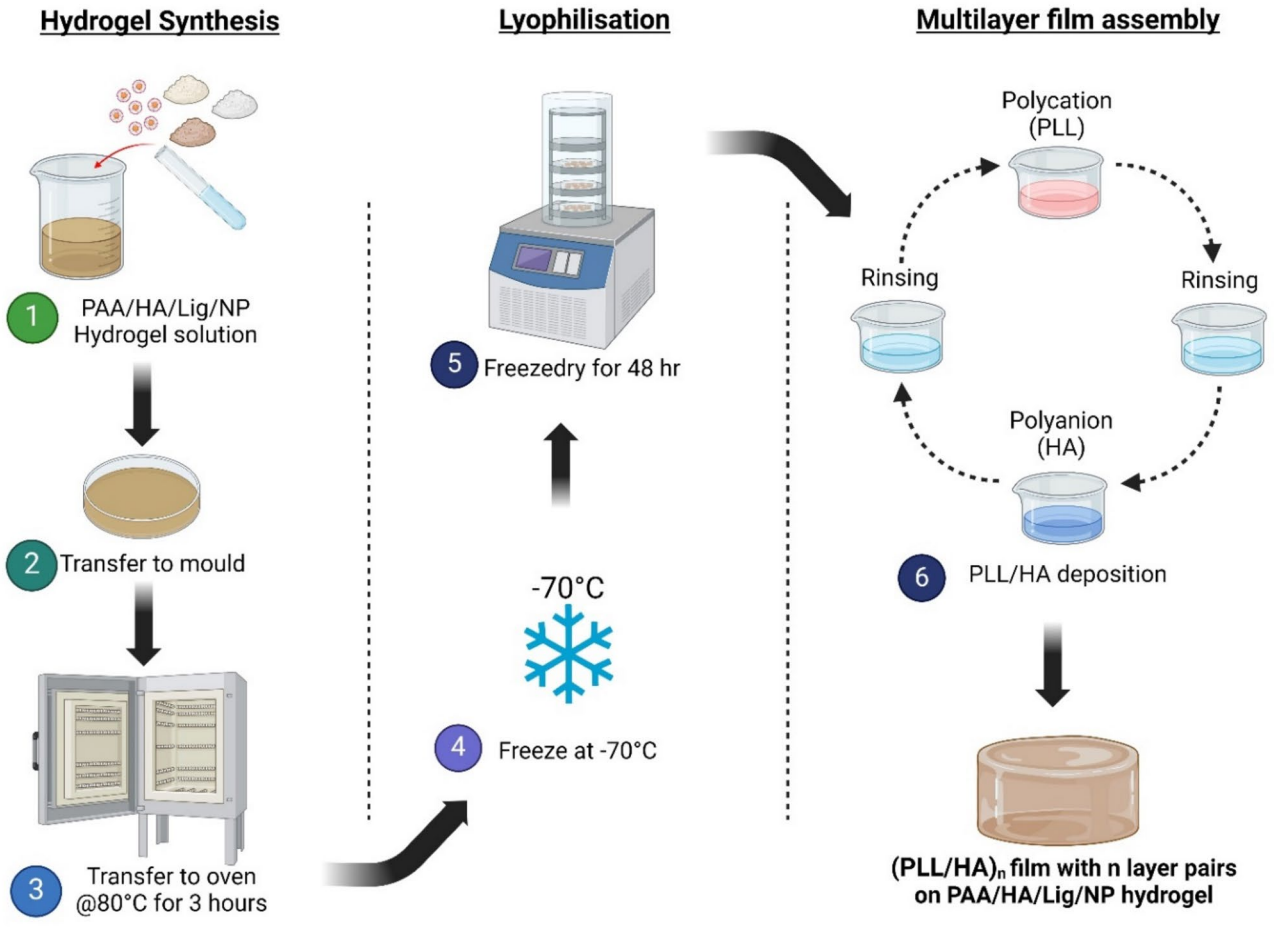

Fig. 1. Schematic of hydrogel preparation steps with LBL film assembly. In steps 1–3 the initial hydrogel material containing AA, HA, Lignin and PEDOT:HA nanoparticles is synthesised. In steps 4–5 the hydrogel is frozen and then lyophilised to form porous scaffolds. Finally, in step 6 the scaffold is dipped alternatively in PLL and HA solutions, rinsing between each step, to form a multilayer film.

Film growth analysis

To quantify the film growth process on the surface of the hydrogels PLL^{FITC} was employed to measure the fluorescence intensity of each layer. Layers were built on the surface of the hydrogel by sequential deposition of PLL^{FITC} (instead of PLL for this experiment) and HA by dip coating as described in Section "Preparation and multilayer deposition of polyelectrolyte solutions". The cross-section of the scaffold was imaged through fluorescence microscopy using the ImageXpress Micro Spinning Disc Confocal High-Content Imaging System (Molecular Devices). ImageJ software was used to calculate the thickness of each coated scaffold.

Swelling analysis

Initially, scaffolds were dried in a vacuum oven at 60 °C until fully dried (2 days). To get the dry weight (Wd) of the samples, they are initially weighed prior to swelling and then placed in a vial containing 10 mL of PBS. At specified intervals, the samples are removed from the PBS, dried of loose solvent and weighed to get the wet weight (Ws) values of the samples. These values were measured up to 2 days and the swelling degree was determined by the following:

$$\frac{Ws - Wd}{Wd} * 100 \tag{1}$$

Contact angle

Following the deposition of each PLL and HA layer, water contact angles were measured using an in-house contact angle measurement system. Contact angles were determined from each image using ImageJ.

Morphological analysis

To obtain a visual image of morphology and film formation, SEM was employed using the Hitachi SU70 SEM at 3 kV. Following synthesis and coating, the hydrogels were lyophilised, and gold sputtered to allow effective imaging.

Mechanical analysis

Unconfined compression tests were carried out using an IMADA Force–Displacement Measurement unit to observe the effect of multilayer formation on the mechanical characteristics of the scaffolds. Swollen Scaffolds were cut into circular discs with a diameter of 10 mm and a height of 3 mm. A speed of 1 mm/min was used for compression of the samples between two circular plates and at least three runs were carried out on each sample, with the mean ± standard deviation presented in the results. The equations used to determine the stress and strain values of the samples from the data obtained were as follows:

$$Stress = \frac{F}{A} \tag{2}$$

$$Strain = \frac{\Delta l}{l_0} \tag{3}$$

F denotes the force (N), A is the cross-sectional area of the scaffold (m^2), l_0 is the original height of the scaffold (mm) and Δl is the change of height recorded in the scaffold (mm).

The compressive strength was calculated from the results and the Young's moduli of the scaffolds were calculated from the slope of the initial linear region of the stress and strain curve.

In vitro cytocompatibility assessment

L929 fibroblast cells (ATCC, USA) were cultured using DMEM complete medium with 1% streptomycin-penicillin, 10% FBS and 1% L-glutamine (all from Sigma Aldrich, Ireland) in a humidified atmosphere, at 37 °C with 5% CO_2. Media was replaced twice a week until the cells reached 80% confluence before subculturing or testing. To sterilise the hydrogels, they were exposed to UV radiation for 2 h and then they were allowed to swell to equilibrium in cell culture media before cell experiments. Cells were seeded onto scaffolds at a density of 50,000 cells per sample/ well and all wells were supplemented with 1 mL of DMEM and incubated overnight. Controls were used in each case, consisting of wells containing just cells, without the presence of scaffolds.

Alamar Blue cytotoxicity assay (Fisher Scientific, Ireland) was used to analyse any cytotoxicity in the scaffolds. Each day, a 10% volume of Alamar blue was added to each of the wells and incubated for 4 h before fluorescence readings were taken in 96-well plates using the SynergyMx (BioTek, UK) at a wavelength of 540/590 nm. Readings were taken at 24, 48 and 72 h post cell seeding.

LIVE/DEAD cell analysis was conducted on the scaffolds following the aforementioned cell culture procedure, after 72 h after culturing. L929 fibroblast cells were stained with Calcein AM and Propidium Iodide (Sigma Aldrich) to stain live (green) and dead (red) cells respectively. Morphological analysis of the cells was also conducted after 72 h of culture. Cells were fixed using 4% paraformaldehyde (PFA) and then stained with NucBlue™ and ActinGreen 488 (Invitrogen). ImageXpress Confocal High Content Imaging System (Molecular Devices) was used to image the stained cells and images were processed and analysed using ImageJ (FIJI) software.

Conductivity analysis

Conductivity analysis was measured by first completing resistivity measurements with an Ohm meter using the two-probe method. Then the conductivity was calculated using Pouillet's law:

$$\sigma = \frac{l}{RA} \tag{4}$$

where σ denotes the conductivity, l is the sample length, R is the resistivity measured, and A is the cross-sectional area of the sample.

Effect of varied nanoparticle addition
Once the coating combination with preferred characteristics is determined, additional testing was carried out on three hydrogels utilising this coating, with varied nanoparticle addition percentage. Hydrogels containing no nanoparticles, 0.5% nanoparticles, 1% nanoparticles and 2% (w/v) nanoparticles were analysed with conductivity testing, mechanical testing and biocompatibility testing.

Statistical analysis
Generally, experiments were completed in triplicate and data obtained throughout the results section is presented as mean ± SD (Standard Deviation). One-way analysis of variance (ANOVA) was used, with an additional Turkey's multiple comparisons test to determine statistical significance between results. A p value of < 0.05 was deemed statistically significant.

Results

Structural analysis

FTIR spectroscopy was utilised to analyse the PEM coatings on the HA/AA/LIG hydrogels with HA and PAA and results are shown in Fig. 2. Uncoated hydrogels ($(PLL/HA)_0$) show the characteristic functional groups of its primary composition of PAA, HA, Lignin and PEDOT:HA NPs. For example, a broad stretch can be seen around 3100 cm^{-1} and 3600 cm^{-1} relating to O–H and N–H stretching. Distinct peaks can also be observed at 1700 cm^{-1}, 1165 cm^{-1} and 1045 cm^{-1} relating to the C=O stretching of PAA, C–O–C stretching of saccharides and C–O stretching vibrations in HA. Changed peaks seen in the spectra of the coated hydrogels ($(PLL/HA)_4$-PLL and $(PLL/HA)_8$-PLL) correspond to functional groups mostly from the PLL as that is the final deposited layer. Peaks seen at 1650 cm^{-1} and 1540 cm^{-1} correspond to the amide I and amide II peptides characteristic to the backbone of PLL with the distinct new amide II peak confirming PLL deposition. The peak seen in the uncoated sample at 1045 cm^{-1} relating to the C–O stretching of HA disappears in the coated samples, as PLL does not contribute to a peak at this wavelength, indicating that the surface is indeed coated with PLL. The broad band seen between 3100 cm^{-1} and 3600 cm^{-1} sees an increase in intensity in the coated samples, likely due to hydrogen bonding between the coatings and the hydrogels carboxyl and hydroxyl groups. Changes in peaks at 1700 cm^{-11} and 1400 cm^{-1} for the coated samples, relating to the C=O stretching and symmetric COO^- stretching, likely indicates interactions with the PLL and HA coatings and the scaffold. Results indicate the successful coating of PAA/HA/LIG/PEDOT:HA scaffolds with PLL and HA polyelectrolyte multilayers.

Morphological analysis

The effect of film coatings on the morphology of the scaffolds was examined through SEM imaging. Samples of unmodified scaffolds $(PLL/HA)_0$ and coated hydrogels ($(PLL/HA)_4$-PLL and $(PLL/HA)_8$-PLL) were lyophilised and gold sputtered before visualisation. The properties of PEMs synthesised using weak polyelectrolytes such as poly(l-lysine) and hyaluronic acid are highly dependent of the ionic strength and pH of the polyelectrolyte

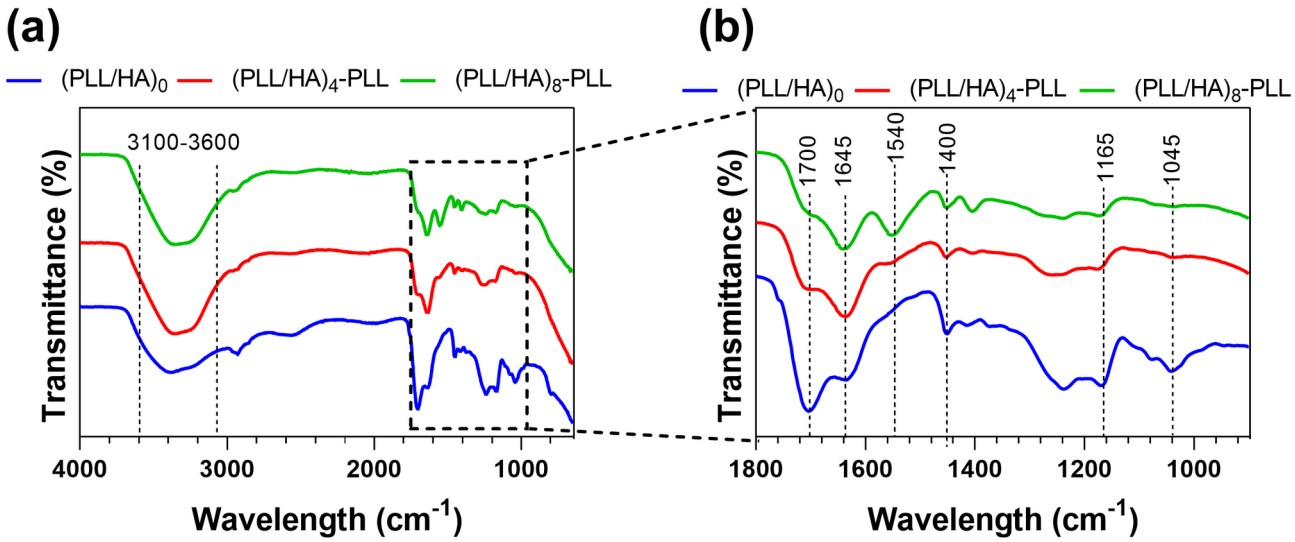

Fig. 2. (**a**) FTIR Spectra of $(PLL/HA)_8$-PLL, $(PLL/HA)_4$-PLL and $(PLL/HA)_0$ scaffolds in the range 650 cm^{-1} to 4000 cm^{-1}. (**b**) FTIR Spectra of the fingerprint region of $(PLL/HA)_8$-PLL, $(PLL/HA)_4$-PLL and $(PLL/HA)_0$ scaffolds in the range 900 cm^{-1} to 1800 cm^{-1}.

solutions[37]. Thus, in order to effectively coat the scaffolds with stable multilayer films, the pH was maintained at pH 6–6.5 in 0.15 M NaCl to maintain a positive charge in the PLL and a negative charge in the HA solutions.

Figure 3 shows the differences in the structure of the surface and cross-section of the hydrogels before and after coating. Samples without any coating $(PLL/HA)_0$ samples have a smooth surface and internal structure with

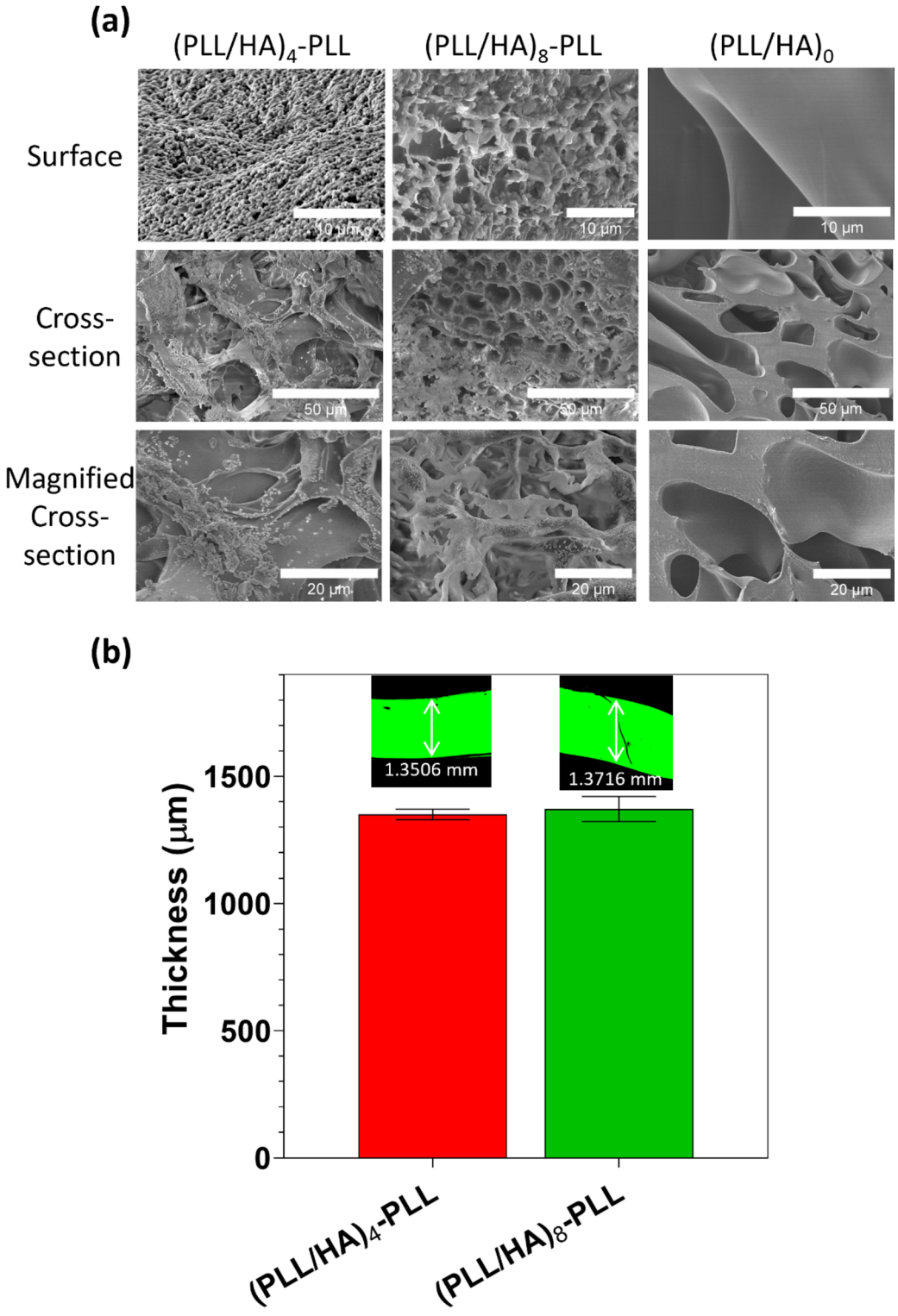

Fig. 3. (**a**) SEM images of the surface and cross-section of hydrogels with $(PLL/HA)_4$-PLL films (left column), $(PLL/HA)_8$ films (middle column) and uncoated hydrogels (right column). (**b**) Effect of the PEM coatings on the scaffold thickness. Initial thickness of swollen scaffold is 1.335 mm before coating. Inset shows fluorescence images obtained of scaffolds following (PLL^{FITC}/HA) coatings.

a clearly visible porous structure. The outside of both coated hydrogels shows a distinctive granular and flaky film and the images also confirm the diffusion of polyelectrolytes into the bulk structure of the scaffolds. This likely occurred when the hydrogel initially came into contact with the PLL solution and the negatively charged HA and PAA hydrogel caused the polycationic PLL to diffuse into the bulk structure of the hydrogel. This may indicate that the first layer formation occurred within the porous hydrogel structure and following this, the sequential deposition steps were formed on the external surface of the scaffold, covering the pores, as confirmed by the SEM images in Fig. 3. The electrostatic charge between PLL and HA occurs due to HA possessing one carboxylic acid per disaccharide unit and PLL having one amino group per monomer repeat unit. This interaction caused the formation of an anchorage layer after the adsorption of the initial PLL layer on the surface on the scaffold[38,39].

To further visualise the presence of films on the surface of the scaffolds, a fluorescently labelled PLL (PLL^{FITC}) was employed in lieu of the polycationic layer to analyse the effect on the thickness of the scaffolds. As seen in Fig. 3b, due to a thin initial thickness and interlayer mixing of PLL^{FITC} and HA, causing the diffusion of PLL^{FITC} across the scaffold, the entire scaffold was caused to fluoresce. An increase in thickness is seen with increased coating layer pairs. The initial swollen scaffold film prior to coating had a thickness of 1.335 mm, meaning that there was a 15.6 µm increase in the $(PLL/HA)_4$-PLL coated scaffold and a 36.6 µm increase in the $(PLL/HA)_8$-PLL scaffold. This indicates the successful PEM coating of up to 8-layer pairs on the surface of the scaffolds.

Swelling analysis and wettability

Swelling analysis was conducted on coated and non-coated scaffolds to determine the effect of PEM coatings on the absorption capacity of the materials and results are shown in Fig. 4a–b. The swelling tests were performed in PBS for 48 h and samples were weighed at predetermined intervals. It was observed that the PEM coated scaffolds exhibited a lower swelling than uncoated samples, likely due to polyelectrolyte diffusion inside the pores, reducing the free space for water absorption. As mentioned in the SEM images of the scaffolds, the polyelectrolytes interpenetrate the pores of the scaffolds, likely leading to their blockage, which would likely have

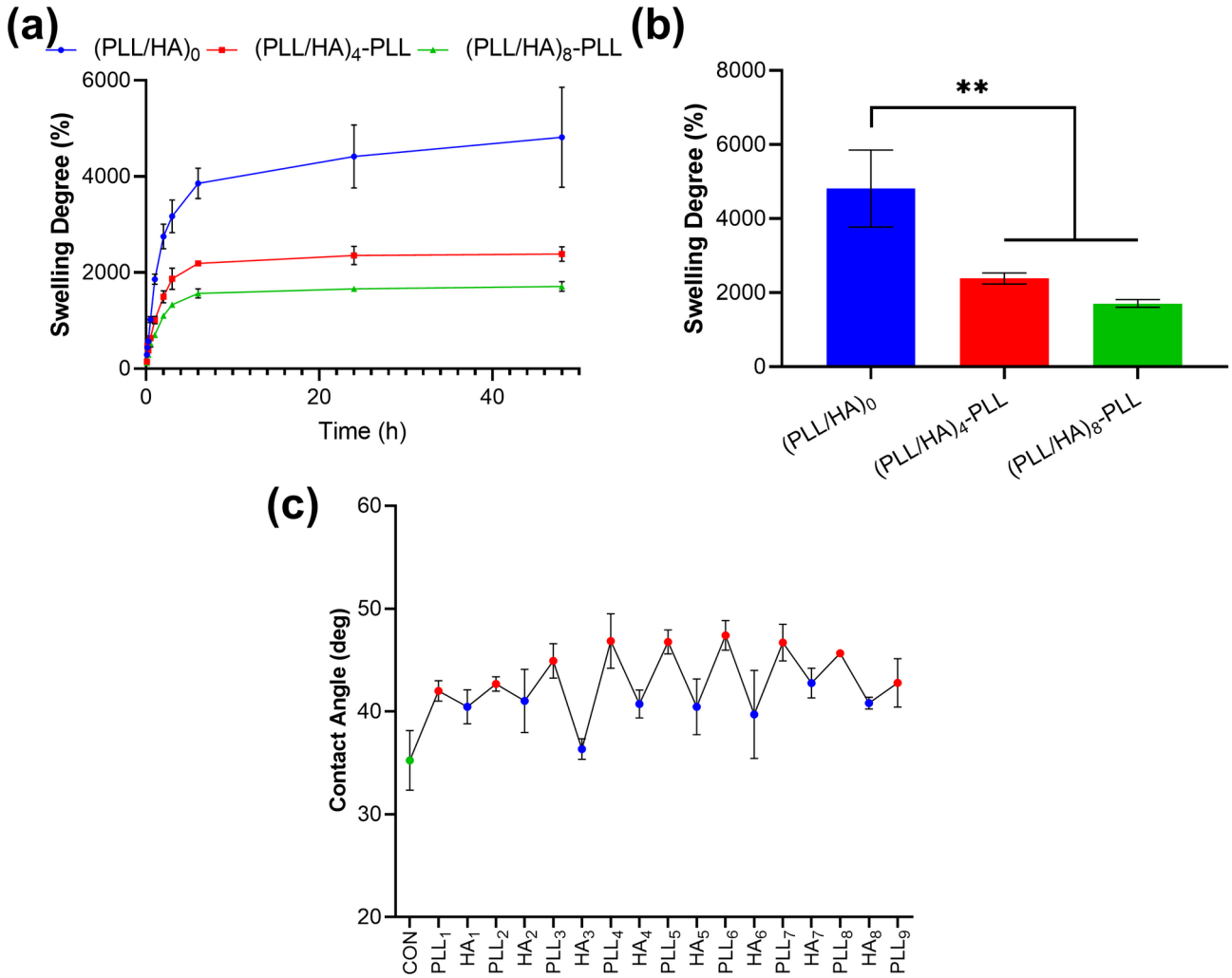

Fig. 4. (**a**) Swelling degree of non-coated and coated samples over 2 days in PBS at 37 °C. (**b**) Overall swelling of non-coated and coated samples at 2 days swelling in PBS at 37 °C (**$p < 0.01$, $n = 3$, mean ± SD). (**c**) Contact angle measurements following each layer coating of PLL and HA on scaffolds.

an impact on their swelling properties. There is a definite reduction in swelling in the coated samples with the non-coated scaffold exhibiting a swelling degree of 4816 ± 1038% and the $(PLL/HA)_4$-PLL and $(PLL/HA)_8$-PLL samples exhibiting 2387 ± 151% and 1712 ± 102% respectively. The presence of PEM coatings on the surface of the scaffolds also likely provides a reinforcement to the structure of the hydrogel, resulting in hydrogel shrinking and a more densely crosslinked network, thus reducing water mobility within the scaffold structure.

Contact angle measurements were also taken at each PLL and HA deposition step to observe the effect of multilayer growth on the wettability of the samples (Fig. 4c) the static water contact angle of the uncoated hydrogels was 35.2 ± 2.9°, which was increased to 41 ± 1° upon one coating of PLL. The contact angle remained increased from its initial state upon sequential layer deposition, indicating that PEM layer deposition increased the hydrophobicity of the scaffolds. The deposition of PLL and HA layers showed high and low contact angles respectively, indicating that the PLL (polycationic) layers were more hydrophobic than the HA (polyanionic) layers. Another possibility is that electrostatic interactions between PLL and HA could also lead to charge neutralisation in the negatively charged scaffolds and thus an increased contact angle is observed upon deposition of PLL. This decrease in wettability correlates with the decrease in swelling in the coated samples caused by the increase in hydrophobicity resulting from the coating of the samples. This also correlated with studies done by Hahn et al. and Yamanlar et al. in which PLL layers yield higher contact angles than HA when built on chitosan and HA surfaces respectively[39,40].

Mechanical analysis

Unconfined compression tests were performed on the samples to determine the effect of PEM coatings on the mechanical characteristics of the hydrogel. The compressive strength and Young's Moduli of the samples were determined from the results obtained, and the values are presented in Fig. 5a–c. Both coated samples demonstrated similar behaviour, however, the Young's Modulus of these samples were significantly lower than the uncoated samples with a Young's Modulus of 22 ± 6 kPa and 20 ± 4 kPa in the $(PLL/HA)_4$ -PLL and $(PLL/HA)_8$ -PLL scaffolds, compared to a Young's Modulus of 34 ± 9 kPa in the uncoated sample. This may be due to the HA and PLL coatings being softer and more elastic than the bulk PAA/HA/LIG hydrogel beneath, leading to a reduced stiffness at lower deformations in the elastic range (as used for Young's Modulus analysis). In contrast to this, the coated samples had a significantly higher compressive strength than the uncoated samples, rising from 129 ± 30 kPa in the $(PLL/HA)_0$ samples to 523 ± 79 kPa and 560 ± 55 kPa in the $(PLL/HA)_4$ -PLL and $(PLL/HA)_8$ -PLL samples respectively. This indicates that the presence of coatings on these samples forms a reinforcement on the surface of the scaffolds for improved stress handling for resistance to higher mechanical loads. The duality of surface softness and resistance to higher mechanical loads could be advantageous for applications that require surface compatibility with tissues while still maintaining durability under higher deformations. The increased overall compressive strength in the coated samples also correlates with the decrease in swelling in the samples. This is likely due to the PEM coatings creating a more densely crosslinked network within the hydrogel, leading to hydrogel shrinking and causing decreased water mobility in the multilayered structure, thus a higher ultimate compressive strength is observed.

Biocompatibility analysis

A very important characteristic needed for tissue engineering materials is the ability for cell adhesion and proliferation on and/or within the structure of a scaffold and this highly depends on the surface characteristics of a material. For cells to adhere to the surface of a material, the material must have adhesion sites for cells to bond to. Despite the biocompatibility and hydrophilicity of hyaluronic acid and polyacrylic acid, both materials have been known to have poor cell adhesion characteristics and need additional modification to improve cell adhesion[41]. PEM coatings were used to provide cell adhesion sites to the scaffolds, and they are characterised in Fig. 6 below. An Alamar Blue proliferation assay was carried out to investigate the viability and proliferation of cells in contact with the coated and un-coated scaffolds. L929 fibroblast cells were cultured with the scaffolds and their fluorescence was measured over the course of 3 days to obtain the cell proliferation which was then compared to a control group containing just cells without the presence of a scaffold. Results can be seen in Fig. 6a in which all samples display a continued increase in fluorescence over the course of a 3-day period. There is no statistical difference between samples at 24 h whereas at 48 h and 72 h a higher fluorescence is seen in the coated hydrogels compared to the control and un-coated hydrogel. The $(PLL/HA)_8$-PLL and $(PLL/HA)_4$-PLL samples at 48 h have an Alamar Blue reduction of 30.1 ± 2.5% and 28.3 ± 6.9% respectively compared to about 22.4 ± 1.6% in the control sample and a much lower 15.3 ± 1.8% in the uncoated sample. At 72 h the $(PLL/HA)_8$-PLL in had a significantly higher proliferation than all other samples at 60.2 ± 2.3% and the uncoated samples had a significantly lower proliferation than all other samples at 41 ± 2.5%. This indicates that the PEM coatings on the samples improve the cell viability, likely due to the ability of cells to adhere and proliferate on the surface of the hydrogels, thus increasing the surface area available for the cells to grow. Two-way ANOVA was employed, and it shows a significant increase in each group each day and any other statistical difference between groups is indicated in Fig. 6a.

In order to determine if the presence of PLL/HA coatings has an influence on the cell attachment and proliferation on the surface of the scaffolds, LIVE/DEAD staining was employed. Control wells containing no scaffolds with just media in a 24-well plate were used for comparison. Images can be seen comparing coated, un-coated and control samples in Fig. 7 with live cells stained in green and dead cells stained with red. Cell viability was calculated from ImageJ and it was 84 ± 10% for the uncoated cells and 88 ± 8% and 87 ± 5% in the $(PLL/HA)_4$-PLL and $(PLL/HA)_4$-PLL respectively, seen in Fig. 7. This demonstrates a slight decrease in cell death in coated samples compared to non-coated samples. Compared with the viability of the control wells at 95 ± 13%, a high cell viability was achieved across the samples. Fibroblast cells display a spindle like or elongated morphology when growing and attaching well to a substrate and thus high circularity indicates poor fibroblast attachment.

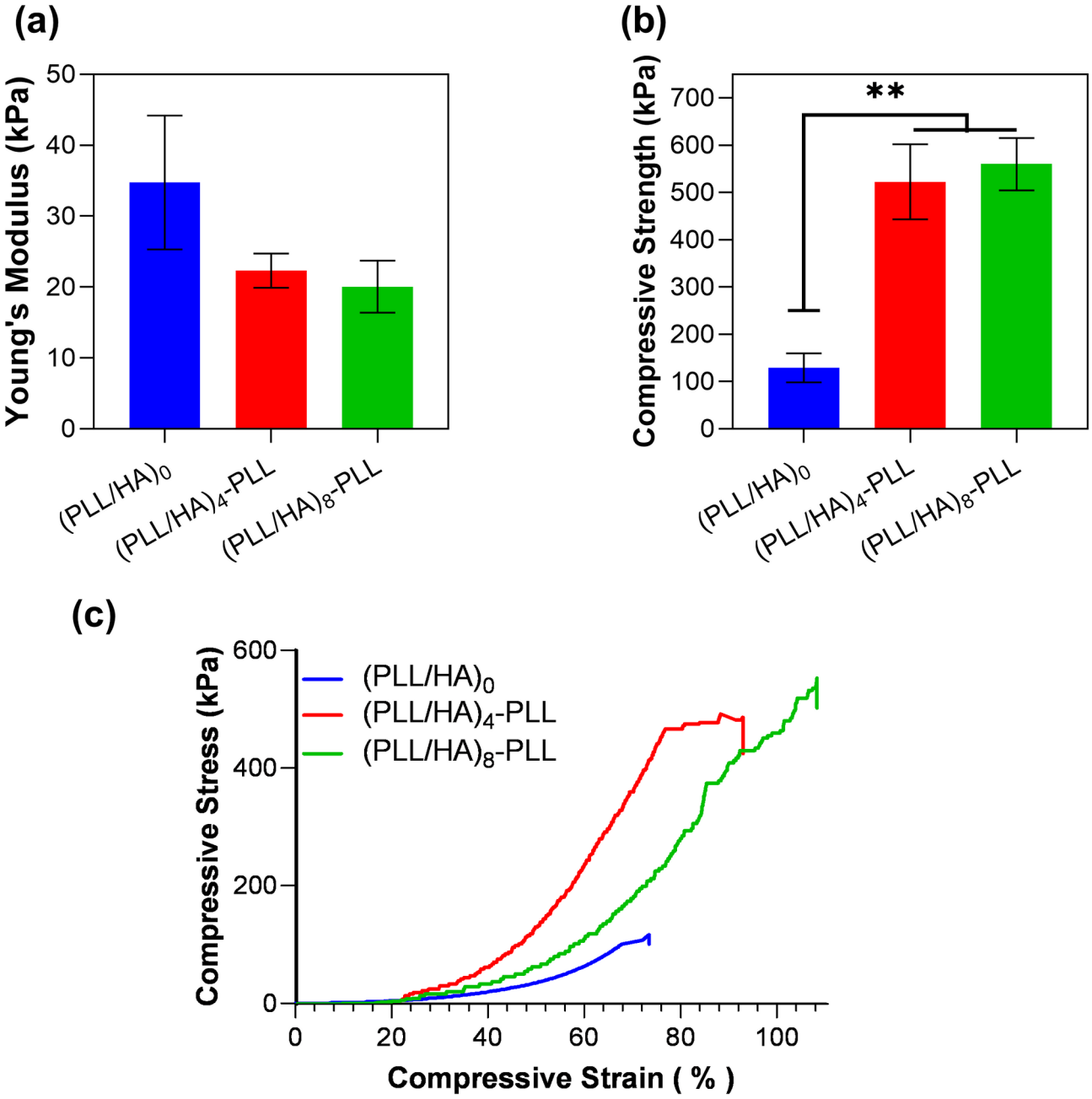

Fig. 5. (**a**) Young's Modulus of coated and uncoated samples (kPa), $^{*}p < 0.05$, n = 3, mean ± SD) is indicated where statistical difference is observed. (**b**) Compressive strength of coated and uncoated samples (kPa), $^{**}p < 0.01$, n = 3, mean ± SD). (**c**) Stress vs Strain graph of coated and uncoated samples.

In previous studies, cell attachment on these scaffolds was poor and fibroblast cells demonstrated a spherical morphology with high circularity, thus the nuclear shape index was used to analyse fibroblast attachment and growth[5,35]. Notably, LIVE/DEAD images for coated scaffolds show improved cell morphology and adherence with the addition of PLL and HA coatings. Uncoated samples display poor cell attachment, fewer cells can be seen in these samples and they have a spherical morphology, with most cells remaining unattached to the scaffolds. However, the coated $(PLL/HA)_4$-PLL and $(PLL/HA)_8$-PLL samples exhibit a significantly improved cell attachment with cells displaying a more characteristic spindle-like morphology and a much higher percentage of cells adhering and proliferating on the surface of the scaffolds. This indicates that the coating of scaffolds in PLL and HA multilayers significantly improves the adherence and proliferation of cells on the surface of PAA/HA/LIG/PEDOT:HA scaffolds.

DAPI/Actin staining was also employed to observe the cellular morphology and distribution on the scaffolds following 72 h and is shown in Fig. 7. Overall, we saw a similar distribution and morphology to the cells imaged with LIVE/DEAD analysis with a spindle like morphology seen in the control and coated samples and a sparse

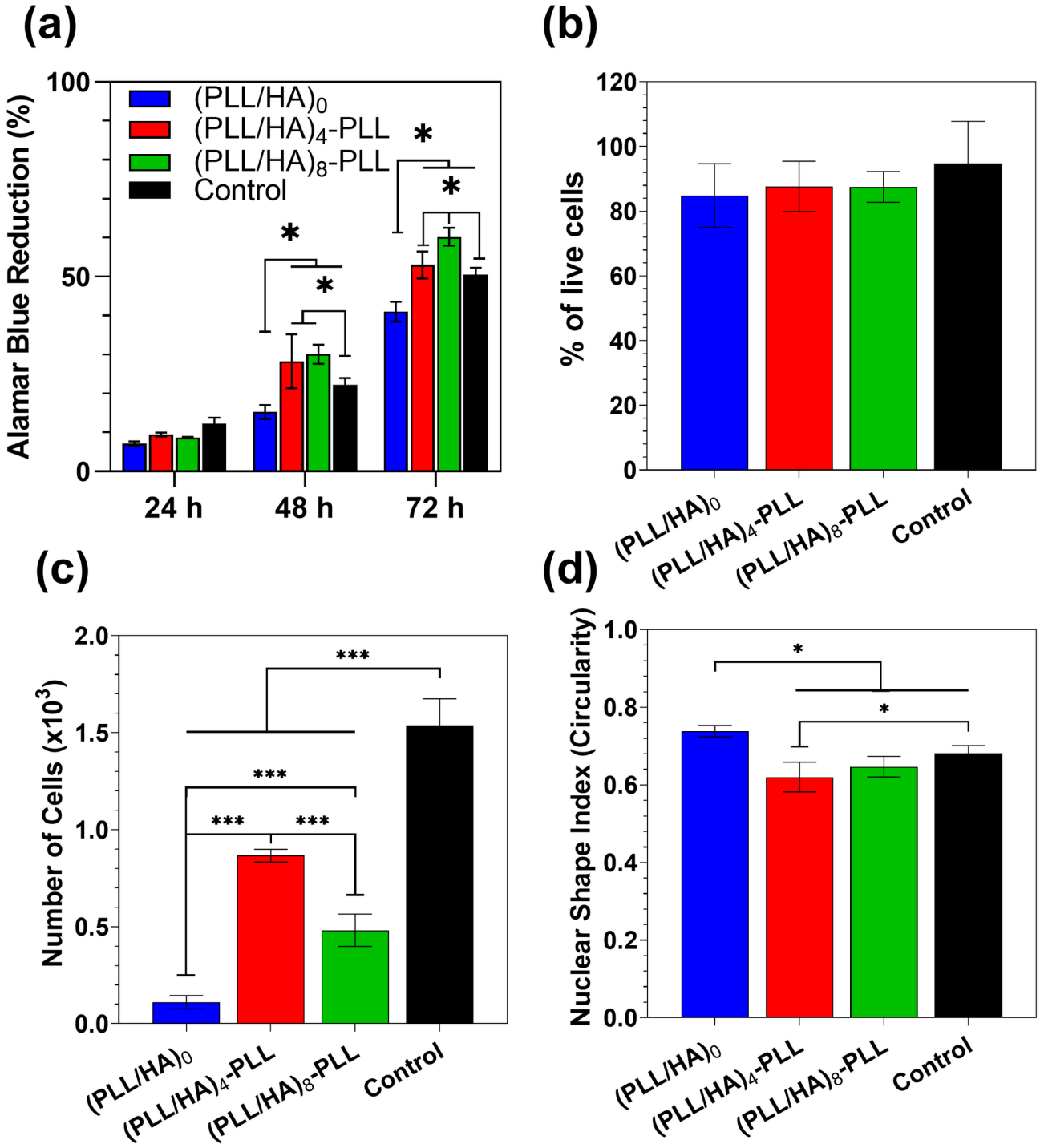

Fig. 6. (**a**) 3-day fluorescence (% reduction of AlamarBlue reagent) of L929 fibroblast cells in coated, uncoated and control (no scaffolds) samples, (*$p < 0.05$, n = 9, mean ± SD) is displayed where a statistical difference is observed. (**b**) Quantification of LIVE/DEAD cell viability quantification, acquired from images in Fig. 7 using ImageJ. (**c**) Density of DAPI stained nuclei per mm^2 of the scaffold surface, calculated from DAPI images in Fig. 7, (***$p < 0.001$, n = 6, mean ± SD). (**d**) Circularity of the cells ($4*\pi*area/perimeter^2$) characterised from Fig. 7 using in-build functions of FIJI ImageJ software, with a nuclear shape index of 1 indicating a circle, (*$p < 0.05$), n = 6, mean ± SD).

distribution and rounded morphology observed in the non-coated samples. Quantification of cells using the stained images observed significantly higher density in the coated scaffolds compared to the uncoated scaffolds with 111 ± 35 cells observed in $(PLL/HA)_0$ increasing to 866 ± 32 and 482 ± 84 in the $(PLL/HA)_4$-PLL and $(PLL/HA)_8$-PLL samples. Similarly, the circularity of the cells was higher in the $(PLL/HA)_0$ sample at 0.74 compared to 0.62 and 0.64 in the coated $(PLL/HA)_4$-PLL and $(PLL/HA)_8$-PLL samples. Overall, the PEM coatings of PLL and

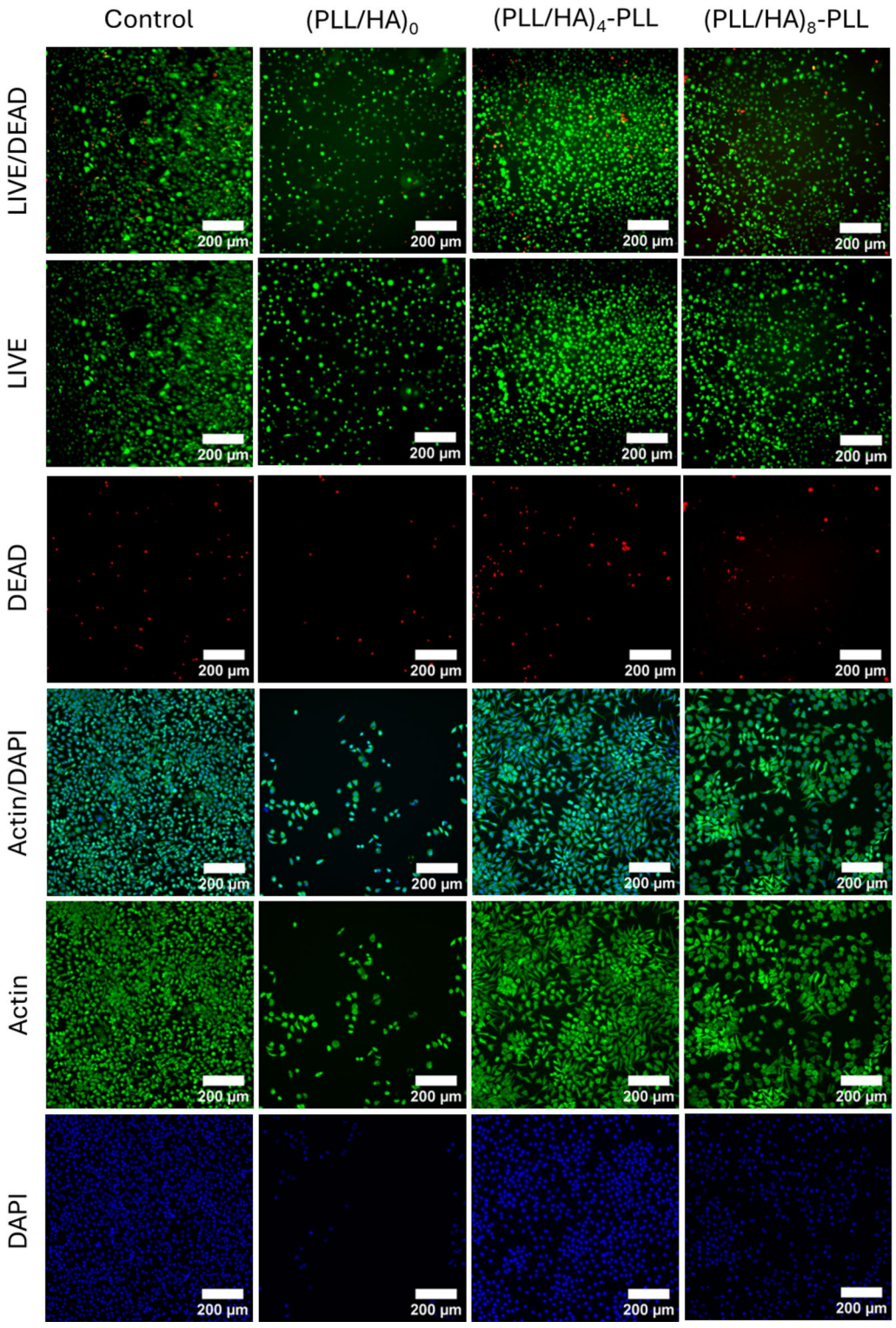

Fig. 7. L929 Fibroblast adhesion following 72 h in a control well (empty well plate with media), on the surface of non-coated PAA/HA/LIG/PEDOT:HA ($(PLL/HA)_0$) and on PAA/HA/LIG/PEDOT:HA scaffolds coated in PLL and HA PEMs ($(PLL/HA)_4$-PLL and $(PLL/HA)_8$-PLL). From top to bottom images depict LIVE/DEAD (green and red) staining, LIVE (green) staining, DEAD (red)staining, Actin/DAPI staining (green and blue), Actin staining (green) and DAPI staining (blue). Scale bar: 200 µm.

HA had a significant improvement on the proliferation and morphology of the cells on the scaffolds compared to previous work[5,34]. One-way ANOVA was used to confirm statistical differences between sample groups.

Analysis of NP variation on scaffold mechanical and conductivity characteristics

Additionally, the authors investigated the effect of varied nanoparticle addition on the mechanical, conductivity and biocompatibility characteristics of coated scaffolds. Following the characterisation of $(PLL/HA)_4$-PLL and $(PLL/HA)_8$-PLL scaffolds, the $(PLL/HA)_4$-PLL PEM coated scaffold was chosen for further characterisation as it had desirable biological and mechanical properties, with a lower coating thickness. Three different nanoparticle (w/v) amounts were added to the $(PLL/HA)_4$-PLL scaffolds (0.5, 1 and 2% (w/v) to obtain three separate sample sets.

The mechanical characteristics were obtained using unconfined compression tests and the Young's Moduli and compressive strengths of the samples are presented in Fig. 8. Previous analysis by the authors have observed lower mechanical characteristics in samples with the addition of nanoparticles[35]. In Fig. 8 a reduction in Young's Modulus can be seen with a higher addition of PEDOT:HA nanoparticles, with a significant decrease seen in the 2% (w/v) samples. A Young's Modulus of only 7.6 ± 2.6 kPa is obtained in the 2%, rising to 22.3 ± 2.4 kPa and 27 ± 9.1 kPa in the 1% and 0.5% samples. An even more significant decrease is observed in the compressive strength of the 2% sample (68.1 ± 12.9 kPa) which is substantially lower than the 522 ± 8 kPa and 585 ± 28 kPa in the 1% and 0.5% samples. This indicates that the mechanical characteristics of the scaffolds majorly suffer with nanoparticle additions higher than 1%. Previous studies found that the PEDOT:HA nanoparticles were prone to agglomerating and so this reduction is likely a result of high nanoparticle ratios agglomerating at higher ratios and acting as barriers to reduce the cross-linking efficiency of the samples which leads to less densely cross-linked samples[35]. This was also observed in the difficulty to crosslink these particular samples during synthesis, with a resulting soft scaffold, unable to maintain a stable structure.

The conductivity of the samples is also presented in Fig. 8 and results indicate that increased addition of nanoparticles into the hydrogel system significantly effects the scaffolds conductivities. The conductivity of the 2% and 1% scaffolds reached $(7.5 \pm 0.4) \times 10^{-5}$ and $(4.7 \pm 0.08) \times 10^{-5}$ S/cm, while there was not much difference between the much lower values of the 0% and 0.5% samples at $(3.5 \pm 0.7) \times 10^{-6}$ and $(8.2 \pm 1.4) \times 10^{-6}$ S/cm. This indicates that percolation is not reached at 0.5% NP addition as it remains at a similar conductivity to the control sample containing no PEDOT:HA nanoparticles. As the conductivity significantly increases at 1% (w/v) nanoparticles, this indicates that the percolation threshold has been met and electrical pathways are formed within the scaffold. In this case, the 2% samples have a significantly higher conductivity to other samples, however, it has poor mechanical and structural properties. Alternatively, there is not a significant difference between the mechanical characteristics of the 0.5% samples and the 1% samples, with the 1% (w/v) samples exhibiting much higher conductivity to the latter, suggesting that this sample may have an optimum balance between conductivity and mechanical characteristics.

Analysis of NP variation on scaffold biological characteristics

Furthermore, the effect of varied nanoparticle addition on the biological characteristics of the coated scaffolds was examined. Alamar blue metabolic assay, LIVE/DEAD staining and Actin/DAPI staining was performed on $(PLL/HA)_4$-PLL scaffolds with 0.5, 1 or 2% nanoparticle additions and compared to samples containing no cells. Results are displayed in Fig. 9. An Alamar Blue metabolic assay was carried out on the samples over 3 days, with results in Fig. 9a. High proliferation was seen in the 0.5% and 1% samples, with the 1% sample showing a higher proliferation to the control sample at day 2 and 3 with a 28.3 ± 6.9 and 53 ± 3.5% reduction compared to a 22.3 ± 1.6 and 50.5 ± 1.8% reduction in the control. All samples increased in proliferation over the three days, except from the 2% (w/v) samples that did not show a significant increase from day 1 to day 2 and day 3. This indicates that this sample inhibits metabolic activity in the cells, possibly due to low stiffness and difficulty for cells adhering to the scaffolds causing quiescence in the cells. Quiescent cells are cells that are healthy but not actively proliferating and one drawback of metabolic assays is that they can only detect actively dividing cells and thus quiescent cells do not contribute to the signal[42,43].

LIVE/DEAD staining was utilised to observe the proliferation and cytotoxicity of the coated scaffolds with varied NP additions. The number of live cells in each sample was obtained through ImageJ processing of images and all samples had cell viability above 87%, similarly to the control. However, significant differences between samples are observed in the overall number of cells and the circularity of the samples, processed using the Actin/DAPI images in Fig. 9e. The 2% samples have a very low cell density of 108 ± 10 cells per mm^2, whereas a significantly higher cell density is observed in the 1% and 0.5% samples at 866 ± 32 and 555 ± 101 cells/mm^2 respectively. Similarly, the circularity of the cells in the 2% samples is around 0.8, compared to 0.62 and 0.58 in the 1% and 0.5% samples. The roundness of the cells, low cell density and the obtained images suggests poor proliferation and attachment of cells in the 2% scaffolds, likely due to poor overall stability and mechanical characteristics in these samples. Alternatively, the 0.5% and 1% samples both demonstrated superior biological characteristics to the 2% sample and would both make suitable scaffolds for biocompatible materials in biomedical applications.

Conclusions

PAA/HA/LIG scaffolds with PEDOT:HA NPs were successfully coated in PEMs of PLL and HA and the effect of multilayer growth on the characteristics of the scaffolds were investigated. SEM, contact angle measurements, FTIR, and fluorescence microscopy were used to confirm the presence and build-up of polyelectrolyte multilayers on the surface of the scaffolds. The swelling degree was reduced upon coating of the scaffolds (from 4816% reduced to 2387% and 1712%) which was likely due to the coatings acting as a reinforcing layer on the surface on the scaffolds, reducing water mobility in the scaffold. This was also indicated by the significant

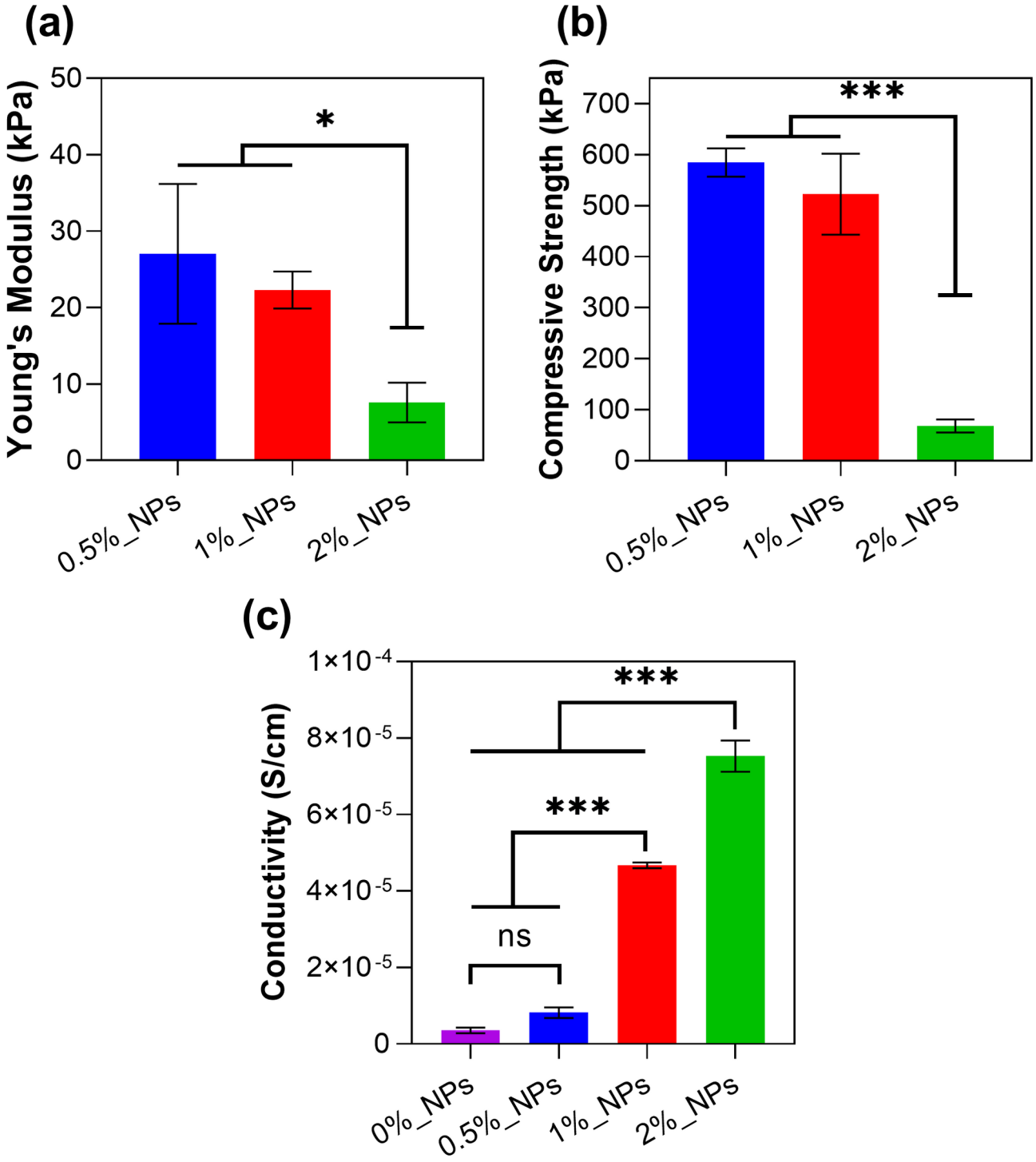

Fig. 8. (**a**) Young's Modulus (kPa) of $(PLL/HA)_4$-PLL scaffolds with varied NP addition (0.5, 1, 2% (w/v)), (*$p < 0.05$, n = 6, mean ± SD). (**b**) Compressive strength (kPa) of $(PLL/HA)_4$-PLL scaffolds with varied NP addition (***$p < 0.001$, n = 6, mean ± SD). (**c**) Conductivity (S/cm) comparison of $(PLL/HA)_4$-PLL scaffolds with no nanoparticles (0%) and with 0.5/1/2% (w/v) addition (***$p < 0.001$, n = 6, mean ± SD).

increase in compressive strength from 129 kPa in the uncoated sample to 524 kPa and 561 kPa in the $(PLL/HA)_4$ -PLL and $(PLL/HA)_8$ -PLL coated samples. Long term swelling studies have been completed on uncoated hydrogels in previous work and were found to be stable for at least 2 months in PBS[35]. The degradation rate of PLL/HA films is dependent on factors such as pH, enzymatic activity, crosslinking and ionic strength of its surroundings in vivo[44]. Thus, future work for coated hydrogels could include long term swelling studies in the environment of the desired application to observe any possible weight loss or degradation. The PEMs also notably increased the biocompatibility of the scaffolds with a much-improved cell density and images display

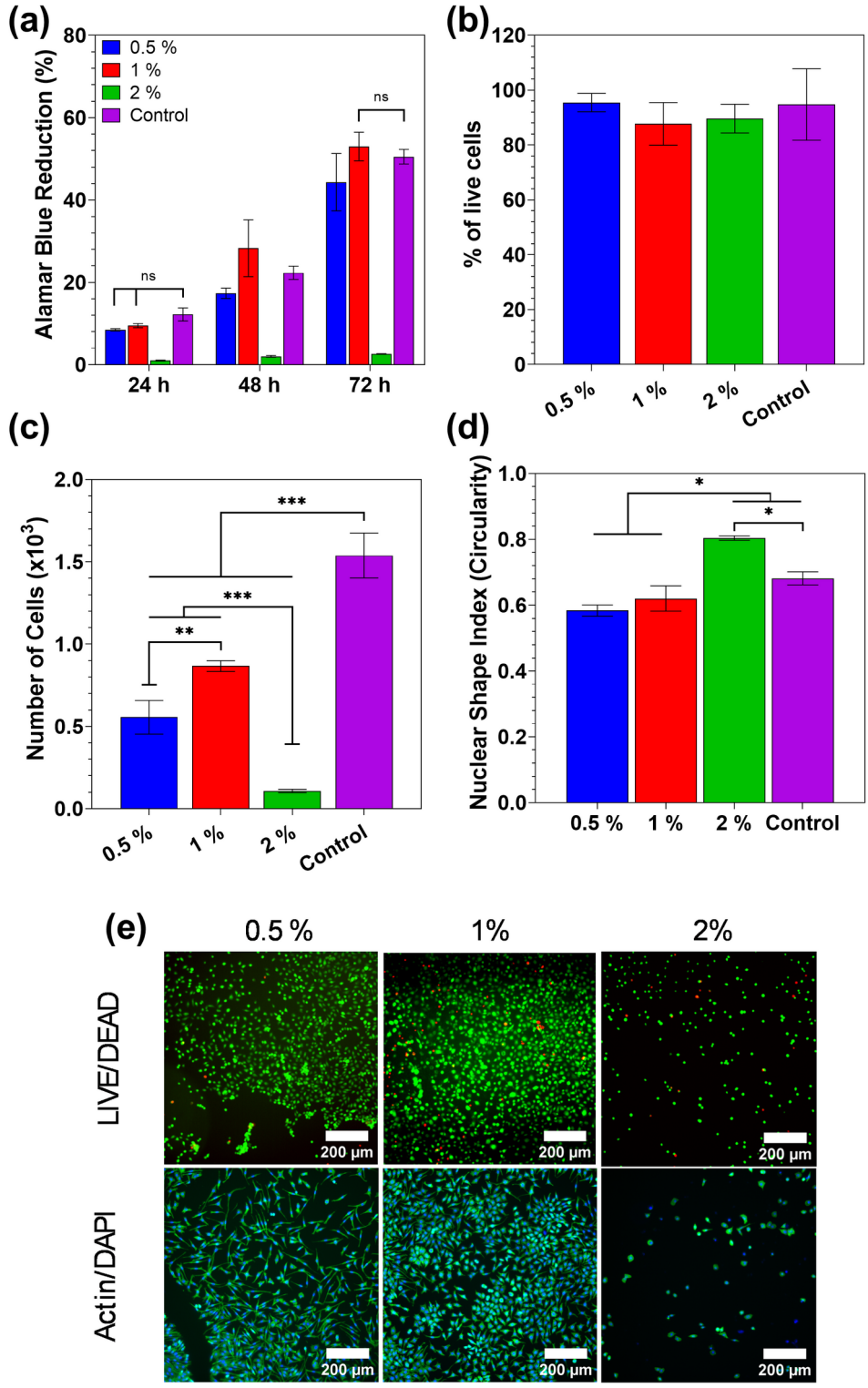

Fig. 9. (**a**) 3-day fluorescence (% reduction of AlamarBlue reagent) $(PLL/HA)_4$ -PLL coated scaffolds with 0.5%/1%/ 2% NPs and control samples (no scaffolds), (ns > 0.05, n = 9, mean ± SD) is displayed where no statistical difference is observed. (**b**) quantification of LIVE/DEAD cell viability quantification, acquired from images in (**e**) using ImageJ. (**c**) Density of DAPI stained nuclei per mm of the scaffold surface, calculated from DAPI images in (**e**), (***$p < 0.001$, **$p < 0.01$) n = 6, mean ± SD). (**d**) Circularity of the cells (4*π*area/perimeter^2) characterised from Fig. 8e using in-build functions of FIJI ImageJ software, (*$p < 0.05$), n = 6, mean ± SD). (**e**) L929 Fibroblast adhesion following 72 h in a control well and on the surface of $(PLL/HA)_4$-PLL coated scaffolds with 0.5%, 1% and 2% NP additives. LIVE/DEAD (green and red) staining can be seen in the top row and Actin/DAPI staining (green and blue) is seen in the second row. Scale bar: 200 µm.

a significantly enhanced cell morphology and proliferation. PEDOT:HA NPs have the potential to affect the coating process as they are negatively charged so they could potentially interfere with HA deposition or alter surface charge distribution. In the contact angle measurements, a distinct increase in contact angle indicates successful coating with the first layer of PAA and a positive surface charge for the initial PLL layer, due to the PLL layer successfully coating the negatively charged scaffold and nanoparticles. The distinct reduction in swelling and SEM images also indicates a complete coating of the scaffold, indicating that PEDOT:HA NPs likely did not significantly disrupt the coating process. The $(PLL/HA)_4$-PLL coated sample exhibited desirable characteristics and thus was chosen for further analysis to determine the most effective nanoparticle addition percentage for an advantageous balance between mechanical, conductive and biological characteristics in this material. Three different nanoparticle additions were considered (0.5, 1 and 2% (w/v)) and characterised. The addition of 2% (w/v) nanoparticle addition had a positive effect on the conductivity of the samples, however, it negatively affected the mechanical and biological characteristics of the scaffolds, leading to a very soft and unstable scaffold, with poor cell adhesion and proliferation, despite PEM coating. Conversely, the 0.5% and 1% samples displayed significantly higher mechanical characteristics reaching a compressive strength of 522 kPa and 585 kPa as well as good biocompatibility and proliferation. With regards to conductivity, the 1% sample significantly outperformed the 0.5% sample at 4.7×10^{-5} S/cm compared to 8.2×10^{-6} S/cm. In conclusion, the coating of PAA/HA/LIG/PEDOT:HA scaffolds was effective in significantly improving the biocompatibility of these materials for use in biomedical applications. The $(PLL/HA)_4$-PLL coated sample with 1% (w/v) NP additives in particular shows the most desirable balance between mechanical, conductive and biological attributes.

Data availability

All data generated or analysed during this study are included in this published article.

Received: 4 February 2025; Accepted: 21 April 2025
Published online: 10 May 2025

References

1. Luo, Y. et al. From crosslinking strategies to biomedical applications of hyaluronic acid-based hydrogels: A review. *Int. J. Biol. Macromol.* **231**, 123308. https://doi.org/10.1016/j.ijbiomac.2023.123308 (2023).
2. Serafin, A., Culebras, M., Oliveira, J. M., Koffler, J. & Collins, M. N. 3D printable electroconductive gelatin-hyaluronic acid materials containing polypyrrole nanoparticles for electroactive tissue engineering. *Adv. Compos. Hybrid Mater.* **6**(3), 109. https://doi.org/10.1007/s42114-023-00665-w (2023).
3. Murphy, C. A., Serafin, A. & Collins, M. N. Development of 3D printable gelatin methacryloyl/chondroitin sulfate/hyaluronic acid hydrogels as implantable scaffolds. *Polymers* **16**(14). https://doi.org/10.3390/polym16141958.
4. Zamboni, F. et al. Enhanced cell viability in hyaluronic acid coated poly(lactic-co-glycolic acid) porous scaffolds within microfluidic channels. *Int. J. Pharm.* **532**(1), 595–602. https://doi.org/10.1016/j.ijpharm.2017.09.053 (2017).
5. Winters, C., Carsi, M., Sanchis, M. J., Culebras, M. & Collins, M. N. On the design of lignin reinforced acrylic acid/hyaluronic acid adhesive hydrogels with conductive PEDOT:HA nanoparticles. *Int. J. Biol. Macromol.* **273**, 133093. https://doi.org/10.1016/j.ijbiomac.2024.133093 (2024).
6. Serafin, A., Culebras, M. & Collins, M. N. Synthesis and evaluation of alginate, gelatin, and hyaluronic acid hybrid hydrogels for tissue engineering applications. *Int. J. Biol. Macromol.* **233**, 123438. https://doi.org/10.1016/j.ijbiomac.2023.123438 (2023).
7. Collins, M. N. & Birkinshaw, C. Hyaluronic acid based scaffolds for tissue engineering—A review. *Carbohydr. Polym.* **92**(2), 1262–1279. https://doi.org/10.1016/j.carbpol.2012.10.028 (2013).
8. Pino-Ramos, V. H., Duarte-Peña, L. & Bucio, E. Highly crosslinked agar/acrylic acid hydrogels with antimicrobial properties. *Gels* https://doi.org/10.3390/gels7040183 (2021).
9. Bolanta, S. O., Malijauskaite, S., McGourty, K. & O'Reilly, E. J. Synthesis of poly(acrylic acid)-cysteine-based hydrogels with highly customizable mechanical properties for advanced cell culture applications. *ACS Omega* **7**(11), 9108–9117. https://doi.org/10.1021/acsomega.1c03408 (2022).
10. Cai, S. et al. Recent advance in surface modification for regulating cell adhesion and behaviors. *Nanotechnol. Rev.* **9**(1), 971–989. https://doi.org/10.1515/ntrev-2020-0076 (2020).
11. Xu, L.-P., Meng, J., Zhang, S., Ma, X. & Wang, S. Amplified effect of surface charge on cell adhesion by nanostructures. *Nanoscale* **8**(25), 12540–12543. https://doi.org/10.1039/C6NR00649C (2016).
12. Collins, M. N., Cagney, L. & Thanusha, A. V. Hydrogel functionalization and crosslinking strategies for biomedical applications. In *Hydrogels for Tissue Engineering and Regenerative Medicine* (eds Oliveira, J. M. et al.) 105–137 (Academic Press, 2024).
13. Liu, Y. & Guo, Z. Small functional hydrogels with big engineering applications. *Mater. Today Phys.* **43**, 101397. https://doi.org/10.1016/j.mtphys.2024.101397 (2024).
14. Luo, Z. et al. Tailoring hyaluronic acid hydrogels for biomedical applications. *Adv. Funct. Mater.* **33**(49), 2306554. https://doi.org/10.1002/adfm.202306554 (2023).
15. Feng, W. & Wang, Z. Tailoring the swelling-shrinkable behavior of hydrogels for biomedical applications. *Adv. Sci.* **10**(28), 2303326. https://doi.org/10.1002/advs.202303326 (2023).
16. Ahmad, Z. et al. Versatility of hydrogels: From synthetic strategies, classification, and properties to biomedical applications. *Gels* **8**(3). https://doi.org/10.3390/gels8030167.
17. Arredondo, R. et al. Fibronectin-coating enhances attachment and proliferation of mesenchymal stem cells on a polyurethane meniscal scaffold. *Regen. Ther.* **18**, 480–486. https://doi.org/10.1016/j.reth.2021.11.001 (2021).
18. Hum, J. & Boccaccini, A. R. Collagen as coating material for 45S5 bioactive glass-based scaffolds for bone tissue engineering. *Int. J. Mol. Sci.* **19**(6). https://doi.org/10.3390/ijms19061807.
19. Bellucci, D., Scalzone, A., Ferreira, A. M., Cannillo, V. & Gentile, P. Adhesive bioinspired coating for enhancing glass-ceramics scaffolds bioactivity. *Materials* **15**(22). https://doi.org/10.3390/ma15228080.
20. Guo, S., Zhu, X. & Loh, X. J. Controlling cell adhesion using layer-by-layer approaches for biomedical applications. *Mater. Sci. Eng. C Mater. Biol. Appl.* **70**(Pt 2), 1163–1175. https://doi.org/10.1016/j.msec.2016.03.074 (2017).
21. Hartmann, H. & Krastev, R. Biofunctionalization of surfaces using polyelectrolyte multilayers. https://doi.org/10.1515/bnm-2016-0015 (2017).
22. Mott, R. & Priefer, R. Multilayering as a solution to medical device failure. *Colloids Surf. B* **193**, 111154. https://doi.org/10.1016/j.colsurfb.2020.111154 (2020).
23. Liu, J., Qu, S., Suo, Z. & Yang, W. Functional hydrogel coatings. *Natl. Sci. Rev.* **8**(2), nwaa254. https://doi.org/10.1093/nsr/nwaa254 (2021).

24. Madaboosi, N. et al. A "cell-friendly" window for the interaction of cells with hyaluronic acid/Poly-l-lysine multilayers. *Macromol. Biosci.* **18**(2), 1700319. https://doi.org/10.1002/mabi.201700319 (2018).
25. Liu, X. et al. Mesenchymal stem cell interacted with PLCL braided scaffold coated with poly-l-lysine/hyaluronic acid for ligament tissue engineering. *J. Biomed. Mater. Res. Part A* **106**(12), 3042–3052. https://doi.org/10.1002/jbm.a.36494 (2018).
26. Tang, Q. et al. A free-standing multilayer film as a novel delivery carrier of platelet lysates for potential wound-dressing applications. *Biomaterials* **255**, 120138. https://doi.org/10.1016/j.biomaterials.2020.120138 (2020).
27. Lei, H. & Fan, D. Conductive, adaptive, multifunctional hydrogel combined with electrical stimulation for deep wound repair. *Chem. Eng. J.* **421**, 129578. https://doi.org/10.1016/j.cej.2021.129578 (2021).
28. Shuping, W. Neural stem cell proliferation and differentiation in the conductive PEDOT-HA/Cs/Gel scaffold for neural tissue engineering. *Biomater. Sci.* **5**(10), 2017. https://doi.org/10.1039/C7BM00633K (2024).
29. Chen, C., Bai, X., Ding, Y. & Lee, I.-S. Electrical stimulation as a novel tool for regulating cell behavior in tissue engineering. *Biomater. Res.* **23**(1), 25. https://doi.org/10.1186/s40824-019-0176-8 (2019).
30. Rocha, I., Cerqueira, G., Varella Penteado, F. & Córdoba de Torresi, S. I. Electrical stimulation and conductive polymers as a powerful toolbox for tailoring cell behaviour in vitro. *Front. Med. Technol.* **3** (2021).
31. Gao, H. et al. Flexible and multi-functional three-dimensional scaffold based on enokitake-like Au nanowires for real-time monitoring of endothelial mechanotransduction. *Biosens. Bioelectron.* **263**, 116610. https://doi.org/10.1016/j.bios.2024.116610 (2024).
32. Inal, S. et al. Conducting polymer scaffolds for hosting and monitoring 3D cell culture. *Adv. Biosyst.* **1**(6), 1700052. https://doi.org/10.1002/adbi.201700052 (2017).
33. Lu, G. et al. Trade-offs between ion-conducting and mechanical properties: The case of polyacrylate electrolytes. *Carbon Energy* **5**(2), e287. https://doi.org/10.1002/cey2.287 (2023).
34. Winters, C., Carsi, M., Sanchis, M. J., Culebras, M. & Collins, M. N. Electrically conductive lignin reinforced polyacrylic acid/hyaluronic acid scaffolds With PEDOT:HA nanoparticles. *Polym. Adv. Technol.* **35**(10), e6607. https://doi.org/10.1002/pat.6607 (2024).
35. Winters, C., Zamboni, F., Beaucamp, A., Culebras, M. & Collins, M. N. Synthesis of conductive polymeric nanoparticles with hyaluronic acid based bioactive stabilizers for biomedical applications. *Mater. Today Chem.* **25**, 100969. https://doi.org/10.1016/j.mtchem.2022.100969 (2022).
36. Picart, C. et al. Molecular basis for the explanation of the exponential growth of polyelectrolyte multilayers. *Proc. Natl. Acad. Sci.* **99**(20), 12531–12535. https://doi.org/10.1073/pnas.202486099 (2002).
37. Alotaibi, H. F., Al Thaher, Y., Perni, S. & Prokopovich, P. Role of processing parameters on surface and wetting properties controlling the behaviour of layer-by-layer coated nanoparticles. *Curr. Opin. Colloid Interface Sci.* **36**, 130–142. https://doi.org/10.1016/j.cocis.2018.02.008 (2018).
38. Mjahed, H. et al. Micro-stratified architectures based on successive stacking of alginate gel layers and poly(l-lysine)–hyaluronic acid multilayer films aimed at tissue engineering. *Soft Matter* **4**(7), 1422–1429. https://doi.org/10.1039/B801428K (2008).
39. Yamanlar, S., Sant, S., Boudou, T., Picart, C. & Khademhosseini, A. Surface functionalization of hyaluronic acid hydrogels by polyelectrolyte multilayer films. *Biomaterials* **32**(24), 5590–5599. https://doi.org/10.1016/j.biomaterials.2011.04.030 (2011).
40. Hahn, S. K. & Hoffman, A. S. Preparation and characterization of biocompatible polyelectrolyte complex multilayer of hyaluronic acid and poly-l-lysine. *Int. J. Biol. Macromol.* **37**(5), 227–231. https://doi.org/10.1016/j.ijbiomac.2005.11.010 (2005).
41. Zhang, X. et al. Fabrication of adhesive hydrogels based on poly (acrylic acid) and modified hyaluronic acid. *J. Mech. Behav. Biomed. Mater.* **126**, 105044. https://doi.org/10.1016/j.jmbbm.2021.105044 (2022).
42. Rampersad, S. N. Multiple applications of Alamar Blue as an indicator of metabolic function and cellular health in cell viability bioassays. *Sensors* **12**(9), 12347–12360. https://doi.org/10.3390/s120912347 (2012).
43. Madhurantakam, S., Jayanth Babu, K., Balaguru Rayappan, J. B. & Krishnan, U. M. Fabrication of mediator-free hybrid nano-interfaced electrochemical biosensor for monitoring cancer cell proliferation. *Biosens. Bioelectron.* **87**, 832–841. https://doi.org/10.1016/j.bios.2016.09.039 (2017).
44. Urbaniak, T. et al. Layer-by-layer assembly of poly-l-lysine/hyaluronic acid protein reservoirs on poly(glycerol sebacate) surfaces. *Eur. J. Pharm. Biopharm.* **193**, 274–284. https://doi.org/10.1016/j.ejpb.2023.10.023 (2023).

Acknowledgements

This publication has emanated from research conducted with the financial support of Science Foundation Ireland under the SFI Research Infrastructure Programme 21/RI/9831. This work was supported by VIBES project. VIBES is a project funded by the European Commission. This project has received funding from the Bio-Based Industries Joint Undertaking (JU) under grant agreement No. 101023190. The JU receives support from the European Union's Horizon 2020 research and innovation program and the Bio Based Industries Consortium. The BIONEER project is supported by the Circular Bio-based Europe Joint Undertaking and its members under Grant Agreement no 101157779. Funded by the European Union. Views and opinions expressed are however those of the author(s) only and do not necessarily reflect those of the European Union or CBE-JU. Neither the European Union nor the granting authority can be held responsible for them. This article reflects only the author's view and the JU is not responsible for any use that may be made of the information it contains.

Author contributions

C.W. and M.N.C. wrote the main manuscript text and M.C. devised the methodology. All authors reviewed the manuscript."

Declarations

Competing interests

The authors declare no competing interests.

Additional information

Correspondence and requests for materials should be addressed to M.N.C.

Reprints and permissions information is available at www.nature.com/reprints.

Publisher's note Springer Nature remains neutral with regard to jurisdictional claims in published maps and institutional affiliations.